NovJ/NovK Catalyze Benzylic Oxidation of a β-Hydroxyl Tyrosyl-*S*-pantetheinyl Enzyme during Aminocoumarin Ring Formation in Novobiocin Biosynthesis†

M. Pacholec, N. J. Hillson,‡ and C. T. Walsh*

Department of Biological Chemistry and Molecular Pharmacology, Harvard Medical School, Boston, Massachusetts 02115

Received July 6, 2005; Revised Manuscript Received July 30, 2005

ABSTRACT: The bicyclic coumarin ring in the aminocoumarin natural product antibiotics that target bacterial DNA gyrase is assembled from tyrosine by nonribosomal peptide synthetase logic. Tyrosine has previously been shown to be activated and installed as a phosphopantetheinyl thioester on the thiolation domain of NovH and then hydroxylated on the benzylic carbon by the heme protein NovI, generating β-OH-Tyr-*S*-NovH. This aminoacyl-*S*-protein is the substrate for the next two orfs, *Streptomyces sphaeroides* NovJ and NovK, that have now been expressed in and purified from *Escherichia coli* as a J_2K_2 heterotetramer. NovJ/NovK use NADP as an electron acceptor to oxidize the β-OH of the tyrosyl moiety to yield the tethered β-ketotyrosyl-*S*-NovH. The enol tautomer is the form that predominates in the subsequently cyclized aminocoumarin scaffold. The labile β-ketotyrosyl thioester moiety was identified by hydrolytic release from NovH, analysis by mass spectroscopy, and comparison with a synthetic sample. We also have identified a residue in NovJ that when mutated results in a 50-fold reduction in catalytic activity.

The antibiotics novobiocin, clorobiocin, and coumermycin A_1 target bacterial DNA gyrase with K_Ds of 10^{-8} to 10^{-10} M (*1*). These natural products have in common a 7-hydroxy-2-aminocoumarin core. During biosynthesis, the phenolic 7-OH of the bicyclic aminocoumarin scaffold is L-noviosylated while the 2-NH_2 group is ligated to a prenylated hydroxybenzoate unit (novobiocin and clorobiocin) or to a methylpyrroledicarboxylic acid that links two aminocoumarin moieties (coumermycin). The noviosyl sugar is then methylated at the 4′-OH and acylated at the 3′-OH to produce the mature, active antibiotic (*2*) (Figure 1). The decorated noviosyl sugar is the pharmacophore that is presented by the planar aminocoumarin to the ATP binding site of the GyrB subunit to interdict DNA replication (*3*, *4*).

The molecular logic of enzymatic assembly of the bicyclic aminocoumarin ring system is under study in our group (*5*). These studies are enabled by the DNA sequence determinations of the biosynthetic gene clusters for all three of the aminocoumarin antibiotics, novobiocin, clorobiocin, and coumermycin, by the Heide group in Tubingen (*6*−*8*).

The framework of the bicyclic 7-hydroxy-2-aminocoumarin arises from the common amino acid L-tyrosine (*9*) which gets routed into secondary metabolism in the producer *Streptomyces sphaeroides* by NovH, the first enzyme in the novobiocin pathway. NovH is a didomainal enzyme containing an adenylation (A) domain and a thiolation (T) domain, reminiscent of an initiation module in nonribosomal peptide synthetase assembly lines (*10*−*13*). The A domain of NovH selects and activates L-tyrosine as tyrosine−AMP and then covalently tethers the aminoacyl moiety to the thiol of a phosphopantetheine prosthetic group in the T domain to yield tyrosyl-*S*-NovH (Figure 2).

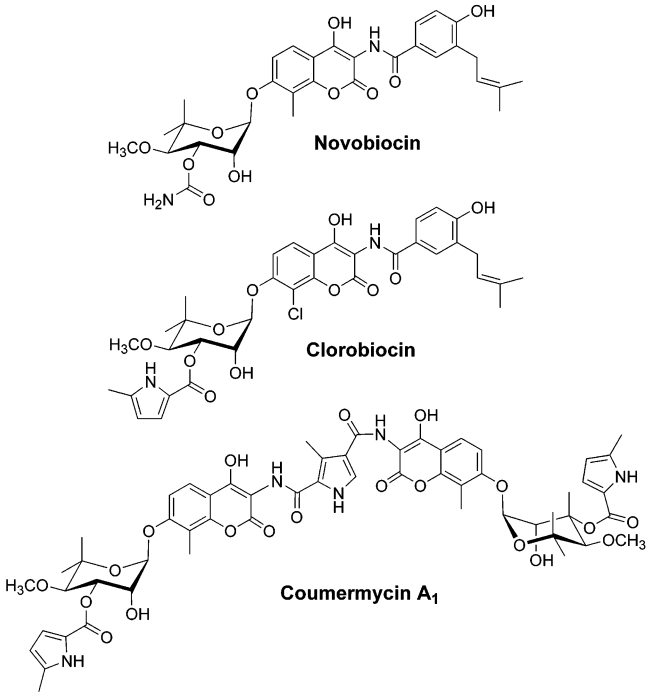

FIGURE 1: Structures of aminocoumarin antibiotics.

It has been our premise that all subsequent modification steps leading to aminocoumarin construction occur on this covalently tethered entity. The heme protein, NovI, acts as a stereospecific monooxygenase on Tyr-*S*-NovH to produce β-OH-Tyr-*S*-NovH (Figure 2) (*5*). Free tyrosine is not a

† We gratefully acknowledge support from National Institutes of Health Grant GM20011 (to C.T.W.), a National Defense Science and Engineering Graduate Fellowship (to M.P.), and a National Science Foundation Graduate Research Fellowship (to N.J.H.).

* To whom correspondence should be addressed. E-mail: christopher_walsh@hms.harvard.edu. Phone: 617-432-1715. Fax: 617-432-0438.

‡ Present address: Department of Developmental Biology, Stanford University School of Medicine, Stanford, CA 94305.

10.1021/bi051297m CCC: $30.25
Published on Web 09/02/2005

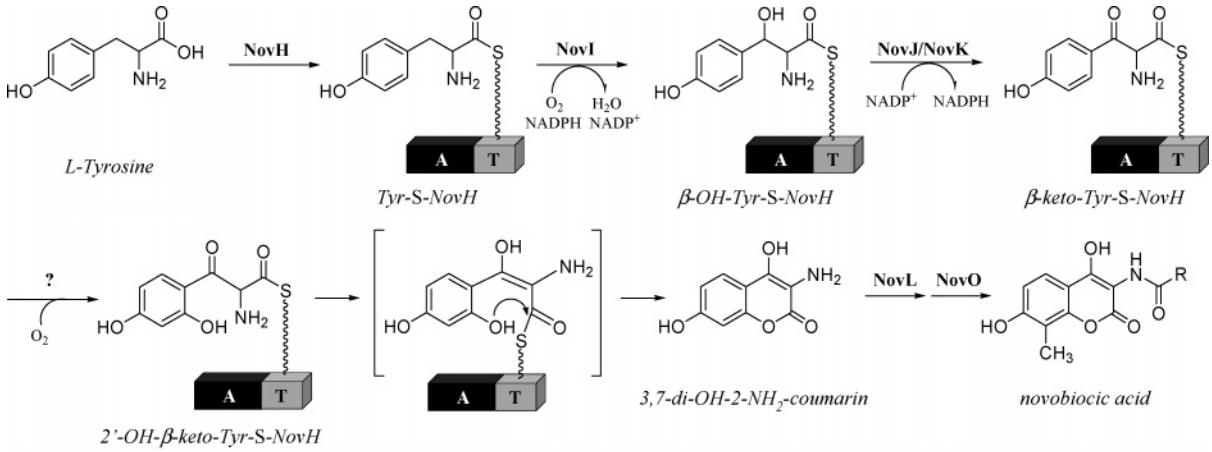

FIGURE 2: Proposed pathway for aminocoumarin ring biosynthesis.

substrate for NovI. Inspection of the oxidation state of the tyrosyl β-carbon in the aminocoumarin scaffold indicates that it is at the ketone oxidation state. We report in this work that the immediately adjacent orfs encoding NovJ and NovK function together as an NADP-dependent oxidase on the NovI product, β-OH-Tyr-*S*-NovH, to produce the β-ketotyrosyl-*S*-NovH acyl-enzyme. The experimental validation of NovJ/NovK activity was not trivial, as the substrate is a labile aminoacyl thioester tethered to the NovH protein that could only be obtained through a single-turnover reaction catalyzed by NovI. The consecutive action of NovI,J,K thus produces a four-electron oxidation of the β-CH_2 of the tyrosyl-*S*-pantetheinyl-NovH.

MATERIALS AND METHODS

Cloning of NovJ and NovK. The genes encoding NovJ and NovK were amplified using PCR from *Streptomcyes sphaeroides* (ATCC 26935) genomic DNA. PCR amplification, performed with *Pfu Turbo* polymerase (Stratagene), was used to generate N- or C-terminally histidine-tagged individual NovJ and NovK constructs (see Supporting Information).

PCR amplification of the NovJ/NovK tandem constructs, using primers that introduced *Nde*I and *Hin*dIII restriction sites (underlined below), was accomplished using primers novJ-1 (5′-GGAGGCGTGCATATGACGAGCCCGGCC-3′) and novK-3 (5′-CAGAAGCTTCCTTTCACGAAGTAGAGGTAC-3′) for a dual histidine-tagged vector (N-His on NovJ and C-His on NovK). The PCR products were gel-purified, digested with *Nde*I and *Hin*dIII, and ligated into the linearized pET28b vector (Novagen), yielding pNovJ(N-His)-NovK-(C-His)-pET28b. For the singly tagged tandem constructs, novJ-1 and novK-2 (5′-CAGAAGCTTCTACCTTTCACGAAGTAGAGGTAC-3′) were used for amplification, ultimately yielding the construct pNovJ(N-His)-NovK-pET16b, with an N-histidine tag on NovJ and no tag on NovK. Similarly, novJ-1 and novK-3 were used in the creation of pNovJ-NovK(C-His)-pET37b, possessing only a C-histidine tag on NovK and no tag on NovJ.

Overexpression and Purification of NovJ and NovK. All expression constructs were transformed into *Escherichia coli* BL21(DE3) competent cells (Invitrogen) for protein overproduction. Transformants harboring the desired constructs were grown in LB supplemented with 50 μg/mL kanamycin (for pET37b and pET28b constructs) and 100 μg/mL ampicillin (for pET16b constructs). Small-scale expression analysis was conducted on individual NovJ and NovK constructs (see Supporting Information).

Transformants harboring the tandem NovJ-NovK constructs [pNovJ(N-His)-NovK-pET16b, pNovJ-NovK(C-His)-pET37b, and pNovJ(N-His)-NovK(C-His)-pET28b] were grown at 37 °C to an OD_{600} of 0.6, cooled to 25 °C, induced with IPTG to a final concentration of 60 μM, and grown for an additional 4−6 h at 25 °C. The cells were harvested by centrifugation (15 min at 6000*g*) and frozen at −80 °C. Thawed cells were resuspended in buffer A [25 mM Tris-HCl (pH 8.0), 400 mM NaCl, 2 mM imidazole, and 10% glycerol], lysed by a French press (three passes at 15000 psi), or a Avestin EmulsiFlex-C5 high-pressure homogenizer (10000−15000 psi), and the resultant cell debris was removed by centrifugation (30 min at 10000*g*). The supernatant was incubated with 0.5−2 mL of Ni-NTA resin (Qiagen) for 2 h at 4 °C. The recovered resin was washed with 50 mL of buffer A and packed into a column, and the protein was eluted using a stepwise gradient of 5−500 mM imidazole. Fractions containing the target protein (judged by SDS−PAGE) were pooled and dialyzed against buffer B [50 mM Tris-HCl (pH 8.0), 100 mM NaCl, 1 mM EDTA, and 10% glycerol] overnight and then in buffer C [50 mM Tris-HCl (pH 8.0), 100 mM NaCl, 1 mM TCEP, and 10% glycerol]. In some cases, a second round of purification was carried out after the initial dialysis step using gel filtration chromatography (HighLoad 26/60 Superdex 200 prep grade; GE Healthcare). The protein was then concentrated, flash frozen in liquid nitrogen, and stored at −80 °C. The protein concentration was determined by Bradford assay (Bio-Rad) and ranged from 2 to 6 mg/L depending on the construct.

Characterization of NovJ/NovK. Reconstitution of NovJ/NovK activity required NovH and NovI (both expressed and purified as previously described) (*5*). Holo-NovH was isolated from *E. coli* coexpressing the *Bacillus subtilis* PPTase enzyme Sfp. Reactions containing 75 mM Tris-HCl (pH 7.5), 5 mM ATP, 10 mM $MgCl_2$, 0.5 mM L-tyrosine, and 1.8 μM [^{3}H]-L-tyrosine (53.4 Ci/mmol) were initiated with holo-NovH to a final concentration of 30 μM and incubated at room temperature for 2 h. NADPH, spinach ferredoxin (Sigma), ferredoxin reductase (Sigma), and NovI were added to a final concentration of 2 mM, 10 μM, 0.1 unit, and 10 μM, respectively. Following a 1 h incubation, $NADP^+$ and NovJ/NovK were added to a final concentration

of 1 mM and 10 μM, and the reaction was incubated for an additional 1 h. The reaction was then quenched with an equal volume of 10% trichloroacetic acid (TCA), and the precipitated protein was pelleted by centrifugation, washed with 10% TCA and twice with 1 mL of water, and redissolved in 150 μL of 0.1 M KOH. The small molecule products tethered to the phosphopantheinyl arm of the NovH carrier protein were released under these conditions by incubation at 60 °C for 5 min. The protein was removed by precipitation following acidification with 5 μL of 50% TFA. The supernatant was analyzed by analytical RP-HPLC [15 min of 100% H_2O and 0.1% TFA followed by a linear gradient of 100% H_2O and 0.1% TFA to 100% CH_3CN over 20 min], and the eluent was analyzed by scintillation counting. In some cases, a small amount of authentic nonlabeled β-ketotyrosine or 2-amino-4′-hydroxyacetophenone (*14*) was co-injected with the reaction mixture.

Assay of NovJ/NovK activity on the (2*S*,3*R*)-β-hydroxy-Tyr-*S*-NAC was performed under a variety of buffer conditions and incubation times. The reaction mixture was evaluated by RP-HPLC in order to detect the presence of a new product peak.

Mass Analysis of the NovJ/NovK Product. A 3 mL reaction mixture containing 75 mM Tris-HCl (pH 7.5), 5 mM ATP, 10 mM $MgCl_2$, 1.0 mM L-tyrosine, and 60 μM holo-NovH was incubated at room temperature for 2 h. Following an additional 1 h incubation in the presence of 2 mM NADPH, 15 μM spinach ferredoxin, 0.2 unit ferredoxin reductase, and 20 μM NovI (final concentrations), $NADP^+$ and NovJ/NovK were added (as described), and the reaction was incubated for an additional 1 h. The reaction was quenched, and the small molecules were released by mild base treatment as described above. The protein was then removed using a spin column (Microcon YM-10; Amicon), and the supernatant was injected onto a RP-HPLC column as previously described in order to separate the reaction intermediates. The eluent was collected, and fractions were concentrated by lyophilization and evaluated by MALDI-TOF-MS. The same procedure was also conducted on the deuterated substrate, (ring-d_4)-L-tyrosine (Cambridge Isotope Laboratories).

Analytical Gel Filtration of NovJ/NovK. Analytical gel filtration was performed using a Superdex 200, 10/300 GL (GE Healthcare) column with a 24 mL bed resin and a buffer system of 50 mM Tris-HCl, pH 8.0, and 100 mM NaCl. A standard curve plotting the log of molecular weight standards versus the calculated K_{av} was generated [log MW = 6.03−3.25 (K_{av}), R = 0.987] using the following protein standards: chymotrypsinogen, albumin, aldolase, catalase, ferritin, and blue dextran (GE Healthcare). This standard curve was used to calculate the observed molecular weight of various NovJ/NovK preparations.

Estimation of the K_D for the heterodimer (NovJK) heterotetramer ($NovJ_2K_2$) equilibrium was performed by curve fitting the observed gel filtration elution profiles with linear combinations of approximate component profiles for each oligomeric species (heterotetrameric, heterodimeric, and monomeric). Only the relevant portion of the elution profile (11.8−16.8 mL), corresponding to 1 mL before the anticipated peak in tetramer elution through 1 mL after the anticipated peak in monomer elution, was utilized in the data fitting. The component profile function was of the following pseudo-Gaussian form: $A \exp(-[(V_e - V_0)/(\tau_0(1 + \tau_1(V_e - V_0)))]^2)$, where A is the amplitude of the profile, V_0 is the standard curve predicted peak elution volume, V_e is the elution volume, τ_0 dictates the Gaussian profile sharpness, and τ_1 dictates (to first-order) how the profile sharpness lessens with increasing elution volume. Of the free parameters, A and τ_0 were allowed to vary between oligomers, but τ_1 was maintained across all oligomers. The relative area under the component profile curves is directly related to the relative amounts of oligomers observed.

Analytical Ultracentrifugation. Sedimentation equilibrium experiments were performed with a Beckman Optima XL-A. NovJ/NovK samples analyzed were at OD_{280}s of 0.7 (58 μM), 0.4 (33 μM), and 0.2 (16.5 μM) in 50 mM Tris-HCl (pH 8.0), 100 mM NaCl, 1 mM TCEP, and 10% glycerol. Scans were collected at 280 and 230 nm at speeds ranging from 11500 to 44000 rpm. Data fitting and analyses were performed using UltraScan 6.0 software.

NovJ/NovK Mutants. Site-directed mutagenesis of NovJ/NovK was performed by a standard method (QuikChange mutagenesis kit; Stratagene) on the vector pNovJ(N-His)-NovK(C-His)-pET28b. Three mutations of *novJ* in the tandem construct were made: S152A using primers 5′-CGGATCATCAACTTCAGCGCCGTGGCCGCGCGCGGC-3′ and 5′-GCCGCGCGCGGCCACGGCGCTGAAGTTGA-TGATCCG-3′, Y164F using primers 5′-GCCGGCCAGAC-CAACTTCGCGACCGCCAAAGGC-3′ and 5′-GCCTTTG-GCGGTCGCGAAGTTGGTCTGGCCGGC-3′, and K168I using primers 5′-CAACTACGCGACCGCCATAGGCGC-GATCGCCGGG-3′ and 5′-CCCGGCGATCGCGCCTATG-GCGGTCGCGTAGTTG-3′ (altered codons are underlined).

Mutants were grown under the same conditions as for the wild-type protein, and activity was assessed as described above.

RESULTS

Expression and Purification of NovJ/NovK. On the basis of small-scale expression analysis for individual NovJ and NovK constructs (see Supporting Information), no suitable conditions for the overexpression of NovJ or NovK were found. Large-scale growth of the corresponding N- and C-terminally tagged proteins under the best expression conditions (37 °C, 60 μM IPTG) yielded no soluble protein. Noting that the stop codon of NovJ overlaps with the start codon of NovK (**ATG**A; NovJ underlined and NovK in bold) in the biosynthetic cluster, the possibility that these two proteins are translationally coupled was tested by cloning the entire two-gene open reading frame in the pNovJ(N-His)-NovK(C-His)-pET28b construct in which both NovJ and NovK were histidine-tagged. Unlike attempts to express NovJ and NovK individually, the heterologous expression and purification of NovJ and NovK was accomplished from this dual His-tagged vector (Figure 3, lane 1).

In an attempt to isolate NovJ and NovK individually, a similar tandem construct with an N-His tag on NovJ but no tag on NovK, pNovJ(N-His)-NovK-pET16b, was constructed and used to express the protein. Surprisingly, both NovJ and NovK were isolated by nickel chelate chromotography despite the fact that only NovJ possessed a histidine tag (Figure 3, lane 2). Furthermore, these two proteins are present at nearly a 1:1 ratio based on densitometry analysis. To demonstrate that the second observed band on the SDS−

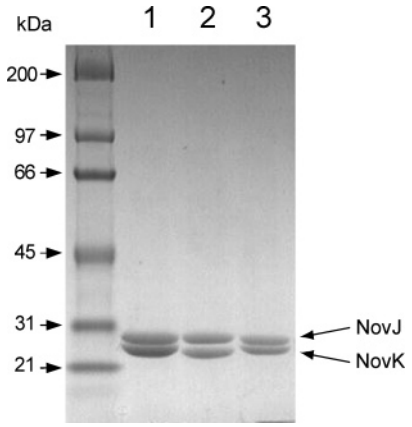

FIGURE 3: SDS−polyacrylamide gel of NovJ/NovK. Lanes: 1, N-His-NovJ and C-His-NovK [purified from pNovJ(N-His)-NovK-(C-His)-pET28b]; 2, N-His-NovJ and NovK [purified from pNovJ-(N-His)-NovK-pET16b]; 3, NovJ(Y164F)/NovK.

PAGE gel was not simply a proteolytic fragment of NovJ, peptide fragment mapping of the top and bottom bands was performed in order to confirm protein identity (Harvard Biopolymers Partner Center for Genetics and Genomics, Cambridge, MA). With 85% and 92% coverage of NovJ and NovK, respectively, the results from peptide fragment mapping confirm that both proteins may be isolated from the pNovJ(N-His)-NovK-pET16b tandem construct and suggest that NovJ and NovK form an association. Similarly, both NovJ and NovK can be isolated from the converse tandem construct, pNovJ-NovK(C-His)-pET37b, in which only NovK is histidine-tagged (data not shown).

Characterization of NovJ/NovK. The in vitro reconstitution of recombinantly expressed NovJ/NovK was accomplished using the aminocoumarin biosynthetic enzymes NovH and NovI in the presence of tyrosine. Radiolabeled small molecules tethered to the NovH didomain are detected by RP-HPLC following hydroxide-mediated release from the thioester of the PCP domain. As previously described (*5*), when NovH alone is incubated with radiolabeled tyrosine in the presence of ATP−Mg^{2+}, only L-tyrosine is detected by RP-HPLC following release from the PCP (data not shown). Upon the addition of the NovI P450 monooxygenase, NADPH, and a heterologous electron transfer system, two new peaks were detected, the NovI product (2*S*,3*R*)-β-hydroxytyrosine (6 min) and its retro-aldol breakdown product 4-hydroxybenzaldehyde (24 min) (Figure 4). In the presence of NovJ/NovK, a new product peak was observed by RP-HPLC at 8.5 min (indicated by an asterisk), accompanied by a reduction in the amount of NovJ/NovK substrate β-hydroxytyrosine and its retro-aldol cleavage product 4-hydroxybenzaldehyde. NovJ/NovK-catalyzed product formation was found to be both substrate and enzyme concentration dependent. In addition, the reaction was dependent on the reducing agent $NADP^+$ but did not require NAD^+ for activity. Indeed, addition of NAD^+ to the reaction mixture resulted in about a 10−20% drop in catalytic efficiency, suggesting that NovJ/NovK may bind NAD^+, but this cofactor is not suitable or is less suitable than $NADP^+$.

To characterize the identity of the NovJ/NovK product peak, an authentic standard of β-ketotyrosine was made synthetically in a previous effort (*14*). Co-injection of this authentic nonlabeled β-ketotyrosine with the NovJ/NovK

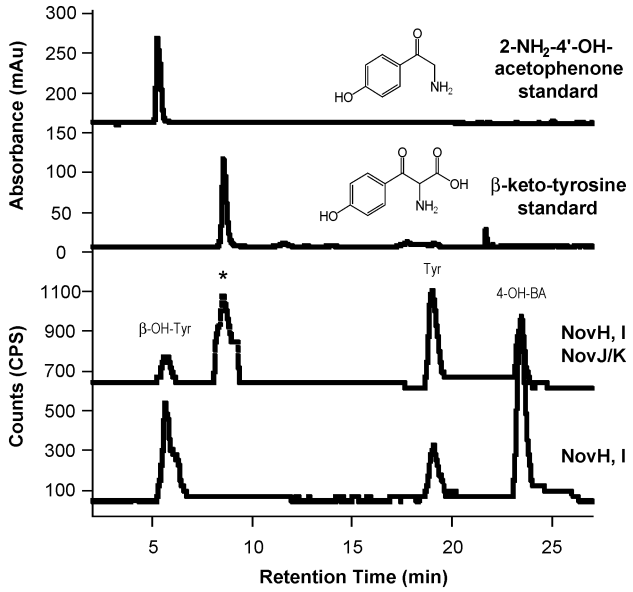

FIGURE 4: Characterization of NovJ/NovK activity by RP-HPLC. Bottom two traces: Radioactive small molecules released from NovH after coincubation with NovI and NovJ/NovK (the asterisk indicates the NovJ/NovK product). Top two traces: HPLC traces of β-ketotyrosine and 2-amino-4′-hydroxyacetophenone authentic standards.

reaction mixture reveals that the two compounds coelute, suggesting that the NovJ/NovK product peak is the expected β-ketotyrosine (Figure 4). Although the identity of the authentic β-ketotyrosine standard was confirmed (*14*), and MALDI-TOF-MS analysis reveals a small peak corresponding to the correct mass, the predominantly observed mass peak corresponds to 2-amino-4′-hydroxyacetophenone, formed by spontaneous decarboxylation of the authentic standard. Presumably, this decarboxylation results during ionization by MS. Indeed, in a similar co-injection experiment with the 2-amino-4′-hydroxyacetophenone standard, no coelution with the NovJ/NovK product peak was observed (Figure 4).

Since the product of the NovJ/NovK reaction remains tethered to NovH, the reaction is single turnover, making characterization of the product challenging. To bypass the need for single-turnover reaction conditions, initially attempts were made to identify the NovJ/NovK product by using the surrogate substrate (2*S*,3*R*)-β-hydroxy-Tyr-*S*-NAC, which was made in a previous synthetic effort (*14*). However, no activity was observed by NovJ/NovK on the *S*-NAC under all conditions tested, indicating that the NovJ/NovK complex does not accept this short-chain mimic and may require interaction with the NovH scaffold to mediate catalysis.

Mass Analysis of the NovJ/NovK Product. A large-scale incubation with ∼180 nmol of NovH was used to isolate enough NovJ/NovK product for mass characterization. Following RP-HPLC separation and concentration, the eluent was subjected to MALDI-TOF-MS. In the case where L-tyrosine was used as substrate, a mixture of peaks was observed, one of which corresponds to the mass of β-ketotyrosine [$C_9H_9NO_4$: calcd, 195.05; obsd, 196.1 $(M + H)^+$]. As expected from previous synthetic efforts (*14*), the decarboxylated amino ketone was also observed during the analysis [$C_8H_9NO_2$: calcd, 151.06; obsd, 152.1 $(M + H)^+$].

To confirm that these observed masses are indeed the NovJ/NovK product and decarboxylated product, a second

large-scale tandem enzyme incubation was performed using (ring-d_4)-L-tyrosine, with the expectation that a new product peak with an increase of 4 mass units would be observed. Indeed, MALDI-TOF-MS of the appropriate HPLC elution fractions yields a new peak [$C_9H_5D_4NO_4$: calcd, 199.08; obsd, 200.1 $(M + H)^+$] corresponding to the mass of β-keto-[ring-deuterated]-L-Tyr. The decarboxylated amino ketone was also observed [$C_8H_5D_4NO_2$: calcd, 155.09; obsd, 156.0 $(M + H)^+$].

Oligomeric State of NovJ/NovK. Given the association of histidine-tagged NovJ with untagged NovK and vice versa during isolation on the nickel affinity matrix, we anticipated that NovJ/NovK would exist as a heterooligomer and investigated this by analytical gel filtration and analytical ultracentrifugation.

Analytical Gel Filtration Chromatography of NovJ/NovK. Injection of a concentrated solution of NovJ/NovK (~155 μM each) yields two peaks, one which elutes with blue dextran corresponding to aggregate protein (8 mL) (Supporting Information) and a second which elutes at 12.80 mL (Figure 5A). On the basis of the generated standard curve, this peak corresponds to a molecular mass of about 114500 Da, which is in very close agreement with the anticipated molecular mass of the NovJ/NovK tetramer (112846 Da). SDS−PAGE gel analysis of the fractions comprising this tetrameric peak reveals an equimolar ratio of NovJ and NovK based on densitometry (average ratio of NovJ:NovK was 1:1.06) (Figure 5B). The analytical gel filtration results therefore confirm that NovJ/NovK exist in a heterotetrameric complex.

Injections of dilute NovJ/NovK solutions onto the column were performed in order to estimate the K_D. Whereas injection of a 22.5 μM solution of NovJ and NovK immediately following dilution yielded no observed change in elution time, a 2 h incubation at 4 °C of this same solution prior to injection results in a slight shift of elution time (12.89 mL), corresponding to a calculated molecular mass of 109.8 kDa (Figure 5A). Similarly, injection of a 2.5 μM solution of NovJ and NovK results in even a further shift in elution time (to 13.11 mL, corresponding to 99 kDa) (Figure 5) following incubation at 4 °C. In addition, a very slight shoulder is observed at an elution time consistent with the expected elution of dimer (indicated by an arrow). These results suggest that some dissociation of the tetrameric complex is occurring during the 4 °C cold room incubation which yields a very small shift in elution time. In the 2.5 μM sample, this shift is more pronounced, and a shoulder is observed. However, even at this low concentration, tetrameric NovJ/NovK is predominant.

To estimate the K_D for the heterodimer−heterotetramer equilibrium, gel filtration elution profile curve fitting was performed. As expected, for the two concentrated samples (155 and 22.5 μM), using exclusively the tetramer component profile yielded the best fit ($R = 0.993$ and 0.990) (Supporting Information, Figures 1 and 2). In contrast, fitting the dilute 2.5 μM sample concurrently with both tetramer and dimer component profiles resulted in the best fit ($R = 0.982$) (Supporting Information, Figure 3). The calculated area under each component profile enabled an estimation of the percentage of heterodimeric and heterotetrameric species present at 2.5 μM. Using these results, the upper limit of the K_D was estimated to be 0.34 μM for $NovJ_2K_2$ dissociation to the dimer NovJK. No monomer component was confidently observed in any of the dilutions tested, suggesting that the K_D for the dimer−monomer equilibrium is substantially lower than that observed for the dimer−tetramer equilibrium.

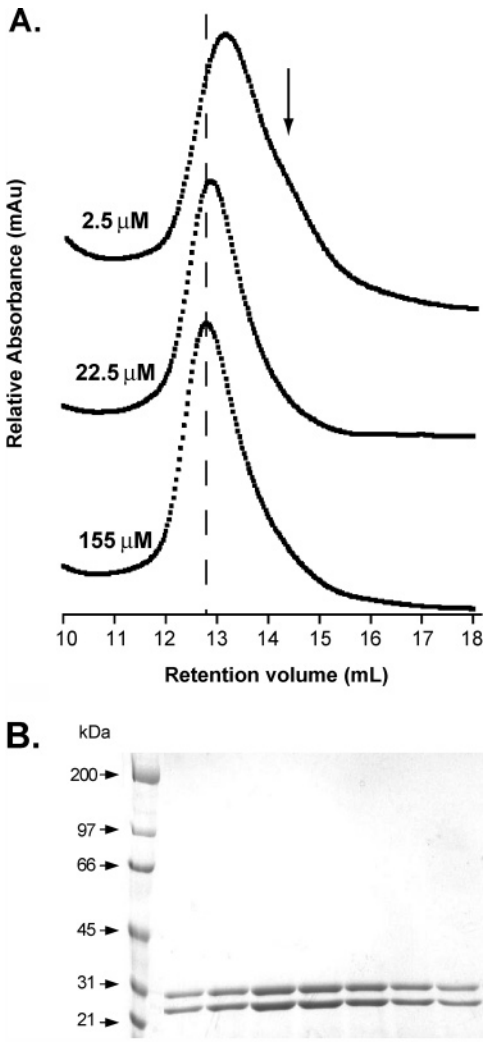

FIGURE 5: Analytical gel filtration chromatography of NovJ/NovK. (A) Analytical gel filtration elution profiles of NovJ/NovK at different concentrations (155, 22.5, and 2.5 μM). The dashed line indicates the predicted elution volume of the $NovJ_2K_2$ tetramer, and the arrow indicates the predicted elution volume of the NovJK dimer. (B) SDS−polyacrylamide gel of fractions collected from gel filtration of 155 μM NovJ/NovK (12−14 mL).

Analytical Ultracentrifugation. The stoichiometry of the NovJ/NovK complex was also assessed by analytical ultracentrifugation. The accumulation of degradation products over time at 4 °C (data not shown) prohibited a reliable calculation of the K_D for the heterodimer−heterotetramer equilibrium, but these ultracentrifigation experiments residually served to corroborate the predominant NovJ/NovK oligomeric species. The accuracy of a given oligomeric model for NovJ/NovK was gauged using two values obtained during the process of fitting of the ultracentrifugation curves, namely, the variance and the percentage number of runs. The variance is a measure of absolute fit error, with a variance less than 1×10^{-4} desirable. The percentage number of runs is a measure of the randomness of the fitting residual (a high percentage indicates randomly distributed error, whereas a low percentage points to systematic error indicative of poor

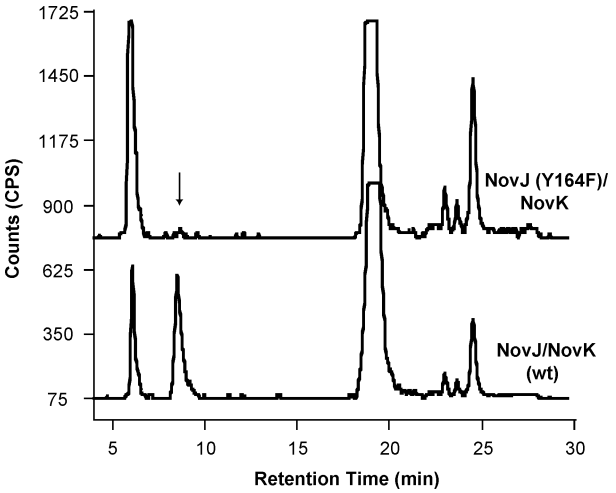

FIGURE 6: RP-HPLC resolution of radioactive small molecules released from NovH after coincubation with wild-type NovJ/NovK or the NovJ(Y164F)/NovK mutant. (The arrow indicates the expected elution time of the NovJ/NovK product, β-ketotyrosine.)

data modeling). An acceptable percentage number of runs is generally over 30%.

A model containing two components, namely, a heterotetrameric $NovJ_2K_2$ species and a degradation product approximately the size of a monomeric NovJ/K, provided a good fit to the experimental data, with a variance of 4.97×10^{-5} and percentage number of runs of 30.7% (overlays and residuals; data not shown). The addition of a heterodimeric component to this model did not improve the fit, consistent with the fact that the lowest concentration tested in the ultracentrifugation experiment was 50-fold greater than the K_D for the dimer−tetramer equilibrium estimated by the gel filtration experiment. An alternate two-component model lacking the heterotetrameric $NovJ_2K_2$ species, containing only the heterodimeric NovJK and the degradation product species, yielded a poor fit with a variance of 1.79×10^{-4} and a percentage number of runs of 14.4% (overlays and residuals; data not shown). These results are consistent with the gel filtration experiments and support heterotetrameric $NovJ_2K_2$ as the predominant oligomeric species.

NovJ/NovK Mutants. A conserved domain search of NovJ and NovK reveals that both proteins also exhibit significant similarity to the family of $NAD(P)^+$ utilizing short-chain dehydrogenases/reductases (SDR) (66% similarity and 47% identity for NovJ and 42% similarity and 30% identity for NovK). Alignment of NovJ/NovK with SDR proteins reveals that NovJ (but not NovK) and its homologues possess the conserved SDR catalytic triad (S152, Y164, and K168). To determine if the NovJ amino acids, S152, Y164, and K168, are analogous to those in SDR enzymes and are involved in catalysis, primer-mediated site-directed mutagenesis was used to mutate these residues individually. Mutant proteins were isolated at purity levels and yields comparable to wild type (Y164F: Figure 3, lane 3) (S152A, K168I: data not shown). Mutation of tyrosine-164 to phenylalanine in NovJ results in an ~50-fold reduction in catalytic activity (Figure 6). Mutation of serine-152 to alanine in NovJ results in a 2−3-fold decrease in β-ketotyrosine product formation. Finally, mutation of lysine-168 to isoleucine did not alter catalytic turnover.

The reduction in catalytic turnover observed with the Y164F mutant indicates that the $NovJ_{Y164}$ residue plays a critical role in the reaction mechanism. The absence of a significant effect on catalytic turnover for the S152A and K168I mutants suggests that NovJ/NovK do not operate through the conserved SDR catalytic triad. It is unclear whether the reaction mechanism is completely different from SDR proteins or if NovJ/NovK use a yet unidentified catalytic triad. These results also suggest that NovK does not have a second independent active site that can function if NovJ is catalytically disturbed. Further study is required to determine the exact mechanism of this β-oxidation chemistry and the exact role of NovJ and NovK in catalysis.

DISCUSSION

The aminocoumarin-based natural product antibiotics, novobiocin, clorobiocin, and coumermycin, act on the same target, the type II topoisomerase bacterial DNA gyrase. This enzyme is also inhibited by the clinically important quinolone class of antibiotics, represented by ciprofloxacin (*15*). The quinolones target sites on the GyrA subunit, resulting in the accumulation of reaction intermediates with both strands of DNA cleaved and tethered covalently to Tyr_{122} of each GyrA subunit in the A_2B_2 heterotetrameric enzyme. DNA replication is stalled in this quinolone−gyrase−doubly cleaved DNA complex, and cell death pathways are activated (*16*).

The aminocoumarin antibiotics instead target the GyrB subunit in the ATP binding site, preventing the ATP hydrolysis required for strand passage of the doubly cleaved DNA intermediate in DNA topoisomer conversion (*17*−*19*). The aminocoumarins have not found a significant clinical niche in human infectious disease therapy because of suboptimal pharmacokinetics, toxicity, and poor penetration into some Gram-negative bacterial pathogens (*20*−*22*). Synthetic variants of aminocoumarins with improved properties have been reported (*23*, *24*), raising the possibility that combinatorial biosynthetic manipulation of the three parts of these molecules, prenylhydroxybenzoate, aminocoumarin, and decorated L-noviose, might lead to improvement in their use as therapeutics.

To that end, an understanding of the molecular logic of how the central 7-hydroxy-2-aminocoumarin scaffold is assembled is a requisite starting point. We have noted previously that antibiotic-producing bacteria and fungi generate nonproteinogenic variants of the common proteinogenic amino acids by diverting part of the primary amino acid pool from ribosomal protein synthesis to nonribosomal peptide synthesis (*25*, *26*). One example of this strategy is the production of β-hydroxytyrosine residues found at positions 2 and 6 of the vancomycin heptapeptide. This process involves the installation of the tyrosyl group as a Tyr-*S*-enzyme on an A-T didomain protein and subsequent stereospecific β-hydroxylation by a dedicated heme protein monooxygenase partner enzyme. In the vancomycin case, β-hydroxytyrosine is then hydrolyzed by a thioesterase, and the free β-hydroxytyrosine is used by the adenylation domains of modules 2 and 6 of the NRPS assembly line (*27*). In novobiocin biosynthesis, the equivalent logic is utilized by aminocoumarin-producing *Streptomycetes* to reroute some of the tyrosine pool onto an A-T didomain protein (NovH). Analogously, a dedicated partner heme protein monooxygenase (NovI) hydroxylates the tethered tyrosyl moiety (*5*).

At this point two differences ensue. First, there are no other NRPS modules in the novobiocin gene cluster. The single amide bond in novobiocin is introduced by a soluble ligase NovL (*28*). Second, the β-OH-Tyr-thioesterified NovH is not hydrolyzed by a companion thioesterase, but rather the β-hydroxytyrosyl moiety is presumed to be the substrate for two additional transformations while tethered to NovH. These transformations would be (1) the β-OH oxidation to the β-keto intermediate, now shown here for NovJ/NovK, and (2) hydroxylation at C_2 of the aromatic ring to facilitate lactonization to the bicyclic aminocoumarin and its release into solution (Figure 2). The covalent thioesterification logic, used for sequestration of a fraction of the free tyrosine pool into the initial steps of antibiotic production, also yields a molecule that is thermodynamically activated to favor the lactonization and release of the newly formed 7-hydroxy-2-aminocoumarin. The versatility of the A-T didomain of NovH as a platform for the consecutive action of NovI,J,K in aminocoumarin construction is unusual and presages use of free-standing A-T didomains in other pathways routing proteinogenic amino acids such as histidine, proline, and isoleucine into secondary metabolites (*25*, *26*, *29*).

The proposed role for NovJ and NovK was first intuited from their location adjacent to *novHI* in the *nov* gene cluster (*novH,I,J,K*) (*6*) and from bioinformatics analysis that indicates that they belong to the nicotinamide-dependent β-keto acid reductase superfamily (*30*). Most intriguingly, we noted homology to a pair of orfs, *bbsC* and *bbsD*, the predicted β-oxidases in anaerobic toluene catabolism (*31*). This raised the possibility of NovJ and NovK acting as a heterooligomer.

While efforts to heterologously express NovJ and NovK individually failed, tandem expression of the two proteins yielded soluble protein. Purification by affinity chromatograpy yielded both NovJ and NovK in stoichiometric amounts, even when only one of the two proteins was histidine-tagged. Analytical ultracentrifugation detected a species with the molecular mass corresponding to a tetramer, and gel filtration confirmed a 110−115 kDa molecular mass with equal amounts of NovJ and NovK, consistent with the heterotetramer $NovJ_2K_2$ (Figure 5). Inspection of residues conserved in NADP-dependent oxidoreductases indicates that NovJ but not NovK have residues predicted to function in catalytic activity. Thus the $NovJ_2K_2$ tetramer may have only two active sites. Mutation of S_{152},Y_{164}, and K_{168} in NovJ resulted in a substantial reduction in β-hydroxytyrosyl benzylic oxidation in the Y_{164}A mutant (Figure 6). Other active site catalytic residues remain to be identified.

The experimental validation of NovJ/NovK β-OH to β-keto oxidation activity was not a trivial undertaking. First, the substrate is a labile aminoacyl thioester tethered to the 60 kDa protein NovH, requiring production of substrate quantities of the Tyr-*S*-NovH. Second, the Tyr-*S*-NovH itself is not a substrate for NovJ/NovK action but requires the catalytic intervention of the monooxygenase NovI to produce the β-hydroxytyrosine form of the aminoacyl moiety tethered to NovH via the phosphopantetheinyl arm. Third, the presumed product of NovJ/NovK action, β-keto-Tyr-*S*-NovH, remains covalently connected to the 60 kDa NovH, and the oxidation state of the aminoacyl moiety cannot be easily analyzed by direct methods.

We had previously shown that radioactive tyrosine (*Tyr) allowed detection of *Tyr-*S*-NovH (*5*). After NovI action the thioester linkage could be hydrolyzed by mild base to release free β-OH-*Tyr, enabling detection by radio-TLC and radio-HPLC analysis and comparison to authentic tyrosine and β-hydroxytyrosine. (Some of the β-OH-*Tyr underwent retro-aldol cleavage to glycine and *p*-hydroxybenzaldehyde during the release workup.) This was the approach we took for the assay of the four protein, NovH,I,J,K, system. Indeed, the release of *Tyr-based radioactivity from such four protein incubations showed a new radioactive amino acid peak, dependent on each of the four proteins (Figure 4). These incubations start with NovH bearing a mixture of *Tyr and β-OH-*Tyr (determined by the efficiency of NovI hydroxylation in any assay) and can produce at most a stoichiometric amount of the 60 kDa β-keto-Tyr-*S*-NovH since the oxidized aminoacyl group remains covalently attached to NovH. Such a system makes the determination of detailed kinetics problematic, allowing only for the detection of product aminoacyl-*S*-enzyme formation.

Our approach was therefore to make an authentic standard for comparison with the radioactive sample released from base treatment of the four enzyme incubations. The unstable nature of free β-ketotyrosine, once released from NovH, makes the molecule quite labile to decarboxylation. It was possible to produce amine-protected β-ketotyrosine esters by adaptation of literature procedures (*32*), but chemical removal of protecting groups led to intractable mixtures of decomposition and condensation products rather than the desired β-keto free amino acid. However, enzymatic deesterification with lipase gave the necessary amino acid standard (*14*) and validated that free β-ketotyrosine was released from NovH. A large-scale enzymatic incubation was performed and gave further confirmation of this product by mass spectrometry.

These results establish the action of $NovJ_2K_2$ as a specific oxidation catalyst on the β-OH site of β-OH-Tyr-*S*-NovH and set the timing of NovJ/NovK action relative to NovH and NovI. Furthermore, this work and our earlier study establish that NovI and NovJ/NovK act in tandem to carry out the four-electron oxidation of the β-methylene carbon of the tyrosyl moiety only when presented on the NovH scaffold. The first two-electron oxidation uses the heme cofactor in NovI and installs one atom from molecular oxygen as the β-OH group. The second two-step oxidation, alcohol to ketone, uses the NADP coenzyme.

The generation of β-ketone functionalities is relatively rare in amino acid metabolism. A notable case is in the formation of levulinate (from enzymatic condensation of the C_2 carbanion of glycine onto the activated acyl carbon of succinyl CoA) where the ketone is analogously adjacent to the amino group. The apposite amino-keto functionality is then utilized in *inter*molecular dimerization to create the pyrrole ring of porphobilinogen and set the first committed step in heme biosynthesis. In the first four enzymes of the novobiocin pathway analyzed here, the α-amino-β-ketone grouping is generated not by aldol coupling but by site-specific oxidation. It will then be used *intra*molecularly, enabling the enolization to the β-OH-enamine tautomer (Figure 2) that is the predominant structure in the final aromatized coumarin bicyclic system.

This work sets the stage for analysis of the subsequent enzymatic steps to complete the 7-hydroxy-2-aminocoumarin core in the novobiocin, clorobiocin, and coumermycin antibiotics, by providing the oxidation state of aminoacyl-*S*-NovH presumably required as a substrate for the later enzymes. In a separate study, we have determined that the *C*-methyl group that appears ortho to the phenol hydroxyl (the 3-position of the tyrosine ring) is not incorporated while intermediates are being processed on the NovH protein scaffold. Instead, C-methylation, at what becomes C8 of the aminocoumarin, happens by NovO action on the novobiocic acid intermediate following NovL but prior to NovM action (Pacholec and Walsh, unpublished results). The most mysterious step remaining is the anticipated C_2 hydroxylation of the β-keto-Tyr-*S*-NovH (for which no candidate enzyme is yet identified) to position the nucleophile for lactonization to the bicyclic aminocoumarin scaffold.

ACKNOWLEDGMENT

We gratefully acknowledge Junhua Tao for synthesis of (2*S*,3*R*)-β-hydroxy-Tyr-*S*-NAC, 2-amino-4′-hydroxyacetophenone, and β-ketotyrosine (*14*). We also acknowledge Huawai Chen for isolation of *S. sphaeroides* genomic DNA.

SUPPORTING INFORMATION AVAILABLE

Additional methods and gel filtration elution profile curve fitting data. This material is available free of charge via the Internet at http://pubs.acs.org.

REFERENCES

1. Maxwell, A. (1993) The interaction between coumarin drugs and DNA gyrase, *Mol. Microbiol. 9*, 681−686.
2. Freel Meyers, C. L., Oberthur, M., Xu, H., Heide, L., Kahne, D., and Walsh, C. T. (2004) Characterization of NovP and NovN: completion of novobiocin biosynthesis by sequential tailoring of the noviosyl ring, *Angew. Chem., Int. Ed. Engl. 43*, 67−70.
3. Lewis, R. J., Singh, O. M., Smith, C. V., Skarzynski, T., Maxwell, A., Wonacott, A. J., and Wigley, D. B. (1996) The nature of inhibition of DNA gyrase by the coumarins and the cyclothialidines revealed by X-ray crystallography, *EMBO J. 15*, 1412−1420.
4. Tsai, F. T., Singh, O. M., Skarzynski, T., Wonacott, A. J., Weston, S., Tucker, A., Pauptit, R. A., Breeze, A. L., Poyser, J. P., O'Brien, R., Ladbury, J. E., and Wigley, D. B. (1997) The high-resolution crystal structure of a 24-kDa gyrase B fragment from *E. coli* complexed with one of the most potent coumarin inhibitors, clorobiocin, *Proteins 28*, 41−52.
5. Chen, H., and Walsh, C. T. (2001) Coumarin formation in novobiocin biosynthesis: beta-hydroxylation of the aminoacyl enzyme tyrosyl-S-NovH by a cytochrome P450 NovI, *Chem. Biol. 8*, 301−312.
6. Steffensky, M., Muhlenweg, A., Wang, Z. X., Li, S. M., and Heide, L. (2000) Identification of the novobiocin biosynthetic gene cluster of *Streptomyces sphaeroides* NCIB 11891, *Antimicrob. Agents Chemother. 44*, 1214−1222.
7. Pojer, F., Li, S. M., and Heide, L. (2002) Molecular cloning and sequence analysis of the clorobiocin biosynthetic gene cluster: new insights into the biosynthesis of aminocoumarin antibiotics, *Microbiology 148*, 3901−3911.
8. Wang, Z. X., Li, S. M., and Heide, L. (2000) Identification of the coumermycin A(1) biosynthetic gene cluster of *Streptomyces rishiriensis* DSM 40489, *Antimicrob. Agents Chemother. 44*, 3040−3048.
9. Bunton, C. A., Kenner, G. W., Robinson, M. J. T., and Webster, B. R. (1963) Experiments related to the biosynthesis of novobiocin and other related coumarins, *Tetrahedron 19*, 1001−1010.
10. Cane, D. E., and Walsh, C. T. (1999) The parallel and convergent universes of polyketide synthetases and nonribosomal peptide synthetases, *Chem. Biol. 6*, R319−R325.
11. Cane, D. E., Walsh, C. T., and Khosla, C. (1998) Harnessing the biosynthetic code: combinations, permutations, and mutations, *Science 282*, 63−68.
12. Marahiel, M. A., Stachelhaus, T., and Mootz, H. D. (1997) Modular peptide synthetases involved in nonribosomal peptide synthesis, *Chem. Rev. 97*, 2651−2674.
13. Schwarzer, D., and Marahiel, M. A. (2001) Multimodular biocatalysts for natural product assembly, *Naturwissenschaften 88*, 93−101.
14. Tao, J., Hu, S., Pacholec, M., and Walsh, C. T. (2003) Synthesis of proposed oxidation-cyclization-methylation intermediates of the coumarin antibiotic biosynthetic pathway, *Org. Lett. 5*, 3233−3236.
15. Pan, X. S., and Fisher, L. M. (1996) Cloning and characterization of the parC and parE genes of *Streptococcus pneumoniae* encoding DNA topoisomerase IV: Role in fluoroquinolone resistance, *J. Bacteriol. 178*, 4060−4069.
16. Drlica, K., and Zhao, X. (1997) DNA gyrase, topoisomerase IV, and the 4-quinolones, *Microbiol. Mol. Biol. Rev. 61*, 377−392.
17. Kampranis, S. C., Gormley, N. A., Tranter, R., Orphanides, G., and Maxwell, A. (1999) Probing the binding of coumarins and cyclothialidines to DNA gyrase, *Biochemistry 38*, 1967−1976.
18. Chatterji, M., Unniraman, S., Maxwell, A., and Nagaraja, V. (2000) The additional 165 amino acids in the B protein of *Escherichia coli* DNA gyrase have an important role in DNA binding, *J. Biol. Chem. 275*, 22888−22894.
19. Gormley, N. A., Orphanides, G., Meyer, A., Cullis, P. M., and Maxwell, A. (1996) The interaction of coumarin antibiotics with fragments of DNA gyrase B protein, *Biochemistry 35*, 5083−5092.
20. Sung, S. C. (1974) Effect of novobiocin on DNA-dependent DNA polymerases from developing rat brain, *Biochim. Biophys. Acta 361*, 115−117.
21. Castora, F. J., Vissering, F. F., and Simpson, M. V. (1983) The effect of bacterial DNA gyrase inhibitors on DNA synthesis in mammalian mitochondria, *Biochim. Biophys. Acta 740*, 417−427.
22. Downes, C. S., Ord, M. J., Mullinger, A. M., Collins, A. R., and Johnson, R. T. (1985) Novobiocin inhibition of DNA excision repair may occur through effects on mitochondrial structure and ATP metabolism, not on repair topoisomerases, *Carcinogenesis 6*, 1343−1352.
23. Ferroud, D., Collard, J., Klich, M., Dupuis-Hamelin, C., Mauvais, P., Lassaigne, P., Bonnefoy, A., and Musicki, B. (1999) Synthesis and biological evaluation of coumarincarboxylic acids as inhibitors of gyrase B. L-rhamnose as an effective substitute for L-noviose, *Bioorg. Med. Chem. Lett. 9*, 2881−2886.
24. Annedi, S. C., and Kotra, L. P. (2001) RU-79115 (Aventis Pharma), *Curr. Opin. Invest. Drugs 2*, 752−754.
25. Chen, H., Thomas, M. G., O'Connor, S. E., Hubbard, B. K., Burkart, M. D., and Walsh, C. T. (2001) Aminoacyl-S-enzyme intermediates in β-hydroxylations and α,β-desaturations of amino acids in peptide antibiotics, *Biochemistry 40*, 11651−11659.
26. Walsh, C. T., Chen, H., Keating, T. A., Hubbard, B. K., Losey, H. C., Luo, L., Marshall, C. G., Miller, D. A., and Patel, H. M. (2001) Tailoring enzymes that modify nonribosomal peptides during and after chain elongation on NRPS assembly lines, *Curr. Opin. Chem. Biol. 5*, 525−534.
27. Hubbard, B. K., and Walsh, C. T. (2003) Vancomycin assembly: nature's way, *Angew. Chem. 42*, 730−765.
28. Steffensky, M., Li, S. M., and Heide, L. (2000) Cloning, overexpression, and purification of novobiocic acid synthetase from *Streptomyces sphaeroides* NCIMB 11891, *J. Biol. Chem. 275*, 21754−21760.
29. Chen, H., Hubbard, B. K., O'Connor, S. E., and Walsh, C. T. (2002) Formation of β-hydroxy histidine in the biosynthesis of nikkomycin antibiotics, *Chem. Biol. 9*, 103−112.
30. Jörnvall, H., Persson, B., Krook, M., Atrian, S., Gonzàlez-Duarte, R., Jeffery, J., and Ghosh, D. (1995) Short-chain dehydrogenases/reductases (SDR), *Biochemistry 34*, 6003−6013.
31. Leuthner, B., and Heider, J. (2000) Anaerobic toluene catabolism of *Thauera aromatica:* the bbs operon codes for enzymes of beta oxidation of the intermediate benzylsuccinate, *J. Bacteriol. 182*, 272−277.
32. Krysan, D. J. (1996) A practical synthesis of α-acylamino-β-keto-esters: acylation of alkyl hydrogen (acylamino)malonates via the $MgCl_2/R_3N$ base system, *Tetrahedron Lett. 37*, 3303−3306.

BI051297M